EFFECTS OF COOLING ON THE PROPAGATION OF MAGNETIZED JETS

A. FRANK,[1] D. RYU,[2] T. W. JONES,[3] AND A. NORIEGA-CRESPO[4]

ABSTRACT

We present multidimensional simulations of magnetized radiative jets appropriate to young stellar objects (YSOs). Magnetized jets subject to collisionally excited radiative losses have not, as yet, received extensive scrutiny. The purpose of this Letter is to articulate the propagation dynamics of radiative MHD jets in the context of the extensive jet literature. Most importantly, we look for morphological and kinematic diagnostics that may distinguish hydrodynamic protostellar jets from their magnetically dominated cousins.

Our simulations are axisymmetric (2.5 dimensions). A toroidal (B_ϕ) field geometry is used. Our models have high sonic Mach numbers ($M_s \approx 10$) but lower fast-mode Mach number ($M_f \approx 5$). This is approximately the case for jets formed via disk-wind or X-wind models—currently the consensus choice for launching and collimating YSO jets. Time-dependent radiative losses are included via a coronal cooling curve.

Our results demonstrate that the morphology and propagation characteristics of strongly magnetized radiative jets can differ significantly from jets with weak fields. In particular, the formation of *nose cones* via postshock hoop stresses leads to narrow bow shocks and enhanced bow shock speeds. In addition, the hoop stresses produce strong shocks in the jet beam, which contrasts with the relatively unperturbed beam in radiative hydrodynamic jets. Our simulations show that pinch modes produced by magnetic tension can strongly affect magnetized protostellar jets. These differences may be useful in observational studies designed to distinguish between competing jet collimation scenarios.

Subject headings: ISM: jets and outflows — MHD — stars: formation

1. INTRODUCTION

The origin of supersonic jets from young stellar objects (YSOs) remains unclear. The current consensus holds that magnetic fields tied to either an accretion disk or the star-disk boundary can launch *and* collimate material into a jet. These "magnetocentrifugal" scenarios have been explored analytically in a variety of configurations including the popular disk-wind (Pudritz 1991; Königl & Ruden 1993) and X-wind (Shu et al. 1994) models. Numerical simulations of magnetocentrifugal mechanisms have shown mixed but promising results. Ouyed & Pudritz (1997) demonstrated that disk-wind models can produce well-collimated jets when the feedback on the disk is ignored. Romanova et al. (1997) have shown that magnetocentrifugal mechanisms can launch winds; however, in their simulations, the winds do not collimate into jets. The potential difficulties involved in turning magnetocentrifugal winds into jets have been noted before. Shu et al. (1995) discussed the slow (logarithmic) rate at which MHD models produce collimation. Ostriker (1997) demonstrated that self-similar MHD disk winds have low asymptotic speeds in cases where they become fully (cylindrically) collimated, and *B* decreases faster than $1/R$ with radius.

Along with these issues, recent numerical studies have shown that pure hydrodynamic collimation can be surprisingly effective at producing well-collimated supersonic jets. Frank & Mellema (1996, 1997) and Mellema & Frank (1998) have demonstrated that isotropic or wide-angle YSO winds interacting with toroidal density environments readily produce oblique inward-facing wind shocks. These shocks can be effective at redirecting the wind material into a jet. If the wind from the central source is varying, this "shock-focusing" mechanism can, in principle, produce jets on the observed physical scales (Mellema & Frank 1998). Similar mechanisms have been shown to work in other jet-producing contexts as well (Peter & Eichler 1996; Mellema & Eulerink 1994; Frank, Balick, & Livio 1996; Borkowski, Blondin, & Harrington 1997).

The variety of available collimation models begs the question of which process actually produces protostellar jets. Observations that can distinguish signatures of different theoretical models are obviously needed. Unfortunately, seeing into the collimation region is difficult. A number of studies indicate that collimation occurs on scales of order $R \lesssim 10$ AU (Burrows et al. 1996; Ray et al. 1996), at or below current observational limits. In addition, the many magnitudes of extinction common for star-forming systems often obscure the innermost region where jets form. Thus, critical observations concerning the formation of the jets will have to come from downstream of the collimation regions, i.e., from the jets themselves.

If the collimation process is MHD dominated, then magnetic fields will remain embedded in the jets as they propagate. In particular, both disk-wind and X-wind models of jet collimation will produce jets with strong toroidal fields. This is evidenced by the fact that while the sonic Mach numbers of the jets may be high ($M_s > 10$), the fast-mode Mach numbers will be low ($M_f \approx 3$; Camenzind 1997). Direct observation of magnetic fields in protostellar jets would help clarify issues surrounding jet origins. Unfortunately, such measurements have generally proved difficult to obtain (Ray et al. 1997).

A promising alternative is look for less direct tracers of strong fields in YSO jets. If jets are produced via MHD processes, dynamically significant magnetic stresses should affect the beam and jet head as they interact with the environment. Thus, the propagation characteristics of protostellar jets may hold important clues to their origins.

[1] Department of Physics and Astronomy, University of Rochester, Rochester, NY 14627-0171; afrank@alethea.pas.rochester.edu.

[2] Department of Astronomy and Space Science, Chungnam National University, Daejeon 305-764, Korea; ryu@sirius.chungnam.ac.kr.

[3] Department of Astronomy, University of Minnesota, Minneapolis, MN 55455; twj@msi.umn.edu.

[4] IPAC, California Institute of Technology, Pasadena, CA 91125; alberto@ipac.caltech.edu.

In this Letter we present the first results of a campaign of radiative MHD simulations of YSO jets. The goal of our on-going study is to search for observable characteristics that distinguish hydrodynamic from magnetohydrodynamic jets. Here we present models that articulate significant radiative MHD effects while also making contact with the extensive bibliography of previous numerical jet studies. Radiative MHD jets are the next logical step in the explication of astrophysical jet dynamics. We have deliberately used simplified initial conditions in our simulations. Our initial setup, similar to those used in past studies, demonstrates new features introduced by the interaction of radiative losses and magnetic stresses in the context of those aspects of jet physics that are well understood.

2. A SHORT HISTORY OF ASTROPHYSICAL JETS SIMULATIONS

Beginning with the work of Norman and collaborators the behavior of axisymmetric jets (2.5 dimensions) without radiative losses has been successfully cataloged and explained (Norman 1993 and references therein). The dynamics of the *bow shock* (which accelerates ambient material), *jet shock* (which decelerates material in the jet beam), and *cocoon* (decelerated jet gas surrounding the beam) have been well studied in these simulations. One should note that these investigations have tended to focus on so-called "light" extragalactic jets in which the density of the material in the jet beam (ρ_j) is lower than that in the ambient medium (ρ_a).

The jets emanating from YSOs are, however, thought to be "heavy" in the sense that the ratio $\eta = \rho_j/\rho_a \geq 1$. Another fundamental difference between extragalactic and YSO jets is the presence in the latter of strong postshock emission from collisionally excited atomic and molecular lines. Thus, while extragalactic jets can be considered "adiabatic," YSO jets must be considered "radiative." Beginning with the work of Blondin, Fryxell, & Königl (1990), the dynamics of radiative jets has been explored in considerable detail (Stone & Norman 1994; Raga 1994; Suttner et al. 1997). These simulations all show that as pressure support is lost, the bow shock/jet shock pair collapse into a thin shell. They also revealed dynamical and thermal instabilities associated with this shell.

MHD simulations of nonradiative jets were first carried out by Clarke, Norman, & Burns (1986) using a strong, purely toroidal magnetic field $\boldsymbol{B} = (0, B_\phi, 0)$. Their results show that "hoop" stresses associated with the radially directed tension force inhibit sideways motion of shocked jet gas. Material that would have spilled into the cocoon is forced into the region between the jet and bow shock, forming a "nose cone" of magnetically dominated low-β gas ($\beta = P_g/P_B = 8\pi P_g/B^2$). Hoop stresses also collapse the beam near the nozzle, producing strong internal shocks. Lind et al. (1989) performed similar calculations, initializing their simulations with a jet in hydromagnetic equilibrium and presenting a more complete exploration of parameter space. They confirmed that nose cones form in jets with low initial β. Kössl, Müller, & Hillebrandt (1990a, 1990b) explored MHD jets with a variety of initial field configurations (poloidal, toroidal, and helical). Cases with significant toroidal fields always developed nose cones. Cases with poloidal fields developed loops with field reversals in the cocoon susceptible to tearing mode instabilities and reconnection. We note studies of MHD instabilities in *just* the jet beam have also been carried out (see, e.g., Hardee, Clarke, & Rosen 1997).

MHD simulations of heavy YSO jets have been carried out by Todo et al. (1992, 1993). These models did *not* include radiative losses. Their jets show similar forms to those simu-

lated by Kössl, Müller, & Hillebrandt (1990a), but Todo et al. (1992) also were able to identify the presence of both slow- and fast-mode shocks in the jet and to present a more quantitative analysis of stability issues.

Very recently, Cerqueira et al. (1997), in a study parallel to ours, have reported the first three-dimensional simulations of radiative MHD jets using an SPH code. Those simulations show results that are similar to what we present below. Our work and that of Cerqueira et al. are complimentary in that very different methods are used. Their study was carried out in three dimensions, while ours is 2.5-dimensional at this point. However, our grid-based axisymmetric simulations have a factor of 10 higher resolution. Especially in radiatively unstable structures, high numerical resolution is important to capture the dynamics properly.

3. INITIAL CONDITIONS

Our simulations evolve the equations of ideal MHD in cylindrically symmetric coordinates (r, z). Since all three components of vector fields are accounted for, the model is 2.5-dimensional. The MHD code used is based on the MHD version of the total variation diminishing method. It is an extension of the second-order finite-difference, upwinded, conservative scheme, originally developed by Harten (1983). The MHD code is described in Ryu & Jones (1995) (one-dimensional version), Ryu, Jones, & Frank (1995) (multidimensional Cartesian version), and Ryu, Yun, & Choe (1995) (multidimensional cylindrical version). The code contains routines that maintain the $\boldsymbol{\nabla} \cdot \boldsymbol{B} = 0$ condition at each time step. However, since the simulations described actually contain only the toroidal component of magnetic field in 2.5 dimensions, $\boldsymbol{\nabla} \cdot \boldsymbol{B} = 0$ is trivially satisfied, although $\boldsymbol{\nabla} \cdot \boldsymbol{B} = 0$ is not enforced in the code.

Cooling is calculated from lookup tables for a coronal cooling curve $\Lambda(T)$ taken from Dalgarno & McCray (1972). Full ionization is assumed, and the cooling is applied in between hydro time steps via an integration of the thermal energy E_t (Mellema & Frank 1998). Tests show the method can recover steady state radiative shocks to within 1% accuracy when the cooling region is resolved. A "floor" on the temperature is set at $T = 10^4$ K. The code has been extensively tested in 1.5 dimensions (Franklin, Noriega-Crespo, & Frank 1997) with and without cooling and against the Uchida et al. (1992) simulations with satisfactory results.

We have performed simulations that compare the evolution of four cases: a nonradiative weak-field jet; a nonradiative strong-field jet; a radiative weak-field jet; a radiative strong-field jet. Since the first three cases have been studied before, our goal was to confirm that the code recovers features seen in previous investigations available in the literature and to extend the sequence into the radiative, strong-field regime.

In each simulation, the jet was driven into the computational domain (128 × 1024) as a fully collimated supersonic/super-fast-mode beam $\boldsymbol{v} = (0, 0, v_z)$. The properties of the jet common to all the simulations were as follows (j, jet; a, ambient medium): $\eta = n_j/n_a = 1.5$; $n_j = 90$ cm^{-3}; $T_a = 1.5 \times 10^4$ K; $v_z = 100$ km s^{-1}. The initial gas pressure in the jet P_j, and hence T_j is varied radially to obtain hydromagnetic equilibrium. Thus, the sonic Mach number $\bar{M}_s$ must be defined as a radial average of $v_j/ [\rho_j/\gamma P_j(r)]^{1/2}$. In all our simulations, $\bar{M}_s \approx 10$ The computational domain spanned $(R, Z) = (8.5 \times 10^{16}$ cm, 6.8×10^{17} cm) with a jet radius $R_j = 2 \times 10^{16}$ cm or 30 grid cells.

In all the simulations, a magnetic field was imposed in the

jet only. The field was purely toroidal. This simplification can be justified on theoretical grounds (Camenzind 1997; Ouyed & Pudritz 1997), since most disk-wind models rely on a dominant toroidal field to produce tightly collimated jets. Hydromagnetic equilibrium between gas and magnetic pressure in the jet was imposed as an initial condition (Priest 1983; Begelman 1997). After choosing a form for $B_\phi(r)$, the equilibrium condition is solved for the initial radial gas pressure distribution $P_j(r)$. In our simulations, we used the same $B_\phi(r)$ and $P_j(r)$ as Lind et al. (1989). As with the sonic Mach number, the Alfvénic Mach number M_a for the jet is a radial average of $B_\phi(r)/(4\pi\rho_j)^{1/2}$. The fast-mode, sonic, and Alfvénic Mach numbers are related by $M_f^{-2} = M_s^{-2} + M_a^{-2}$. For our strong-field simulations, the average initial value of the field is ≈ 100 μG and an average plasma beta ≈ 0.7. It should be noted that this configuration, known as a Z-pinch in the plasma physics community, is almost always unstable to both pinch and kink modes. Since our simulations are axisymmetric we are unable to track kink modes (but see Cerqueira et al. 1997; Todo et al. 1993). The pinch modes are quite important, however, and, as Begelman (1997) has shown, the beam will be unstable to these instabilities when

$$\frac{d \ln B}{d \ln r} > \frac{\gamma\beta - 2}{\gamma\beta + 2}, \qquad (3.1)$$

where γ is the ratio of specific heats. This condition is satisfied for the Lind et al. (1989) initial configurations. We note that since these simulations include radiative cooling, $P(r)$ quickly flattens out as the jet propagates.

4. RESULTS

We first present an equation to estimate the speed of the jet head, v_h (the bow shock), that accounts for magnetic (and gas) pressure effects. We define $P_t = P_B + P_g$ and $\alpha = (R_j/R_h)^2$, where R_h is effective jet head radius over which the ram pressure, $\rho_a v_h^2$, is applied. From one-dimensional momentum balance, ignoring the ambient pressure, we find

$$v_h = v_{ho} \frac{1 - \sqrt{1/\eta\alpha - (P_t/\rho_j v2_j)[1 - (1/\eta\alpha)]}}{1 - (1/\sqrt{\eta\alpha})}, \qquad (4.1)$$

where $v_{ho} = v_j / [1 + (1/\sqrt{\eta\alpha})]$ is the familiar expression for the speed of a "cold," pressureless jet (see, e.g., Dal Pino & Benz 1994), and the remaining terms describe an "enhancement factor" for the head speed due to finite jet pressure. This factor in equation (4.1) is *always greater than or equal to unity*, as we should expect. For the limiting case $\eta\alpha = 1$, equation (4.1) gives $v_h = \frac{1}{2} v_j [1 + (P_t/\rho_j v_j^2)]$. In Figures 1 and 2 (Plates L4 and L5), we present the results of our simulations with $\eta = 1.5$. We will use equation (4.1) to interpret the results presented below.

Case A: nonradiative weak-field jet.—Here the magnetic field is set quite low, so that the Alfvénic Mach number is $M_a \approx 10^4$. Figure 1 shows clearly the well-known bow shock/ jet shock configuration at the head of the jet (Norman 1993). The scale of the bow shock is relatively large because of the postshock thermal pressure. Note, however, that the speed of the jet (100 km s^{-1}) is relatively low compared with extragalactic jets. Thus, the post–*jet*-shock temperature in this simulation is low ($T \approx 10^5$). The pressure in the cocoon is therefore also small compared with extragalatic jet simulations, and only

weak internal waves are forced into the jet beam. Blondin et al. (1990) found a similar result in their comparisons of non-radiative and radiative YSO jet simulations.

Case B: nonradiative strong-field jet.—Here a stronger field is used, so that the Alfvénic Mach number is $\bar{M}_a \approx 7$ ($\bar{M}_f \approx 5$). In this simulation the structure of the jet head has changed dramatically due to dynamical influences of the field. Note the large separation of the jet and bow shocks. As has been described in other MHD jet studies (Clarke et al. 1986; Lind et al. 1989; Kössl et al. 1990a, 1990b), such "nose cone" structures occur because of the pinching effect of the magnetic hoop stresses. Post–jet-shock material, which would otherwise back flow into the cocoon, is forced to remain between the two shocks. The bow shock is accelerated forward, producing higher propagation speeds (note the times at which the images were taken). In previous studies, the acceleration was attributed to the magnetic pressure in the nose cone (Kössl et al. 1990b). We demonstrate below that the increased speed can be better attributed in this case to a cross section effect produced by magnetic pinch forces. Note the strong convergence occurring just beyond the jet nozzle and the reflected shocks in the beam downstream. This occurs due to the pinch instability described in § 3 and has been seen in all MHD jet simulations with strong toroidal fields. We note also that these results look quite similar to the those presented by Kössl et al. (1990b) (see their Fig. 10a).

Case C: radiative weak-field jet.—The magnetic field in this case is the same as case A. Again the standard bow shock/jet shock configuration is apparent. Maps of temperature show that the post-bow/jet shock region is nearly isothermal. The loss of postshock thermal energy reduces the transverse width of the bow shock. Densities behind the shocks become high with compression ratios of ≈ 30 (compared with the value of ≈ 4 obtained in the nonradiative case). Animations of this model show that the structure at the jet head is highly time-dependent, with the region between the two shocks becoming quite thin at times. At late times in the simulation the jet head undergoes the nonlinear thin shell instability (Vishniac 1994), which also has been observed in other radiative jet simulations (Blondin et al. 1990; Stone & Norman 1994). Note again the lack of structure in the jet beam. In both cases A and C the jet heads propagate at a velocity $v_h \approx 53$ km, which compares well with $v_{ho} = 55$ predicted by equation (4.1) for a cold jet (v_{ho}) with $\alpha \approx 1$.

Case D: radiative strong-field jet.—In this simulation the field is the same as for the nonradiative, strong-field jet (case B), and the structure of the jet head is similar to what obtains in that simulation. A narrow bow shock appears some distance ahead of a high-density region associated with the jet shock. Note that the loss of thermal energy behind the shocks has reduced the scale of the bow shock R_h compared with its non-radiative twin. Figure 2 shows the evolution of this simulation at four different times.

For this case the initial collapse of the beam just beyond the nozzle produces a series of strong shocks and reflections in the jet as it propagates down the length of the grid. Figure 2 shows the periodic density enhancements in the beam formed from these reflections. If such features are not a consequence of the imposed axisymmetry, they may have important consequences for the emission characteristics of real YSO jets. Figures 1 and 2 show that a jet shock forms close to the bow shock. The reduced width of the jet shock/bow shock pair is similar to what is seen in the evolution of the weak-field radiative jet (Blondin et al. 1990).

The most important conclusion to be reached from these simulations comes from comparison of the third and fourth panels of Figure 1. For radiative jets, the weak- and strong-field cases look dramatically different from each other in terms of the morphology of the jet head and beam. In the weak-field case there are no shocks in the beam. The strong-field case shows multiple shock reflections (Fig. 2). The head of the weak-field jet is quite "blunt" compared with the strongly tapered strong-field jet. The average propagation speed for the head of the strong-field jet is $v_h \approx 70$ km s^{-1}, a 25% increase over the weak-field case, even though both simulations have the same jet/ambient density ratio, η. The combination of higher shock speeds and strong pinch forces in the radiative strong-field jet produces a compression ratio in the head almost twice as large as in the radiative weak-field case. If these results are borne out in more detailed studies, particularly those in three dimensions, then indirect diagnostics of the presence of dynamically strong fields in jets should exist.

As noted, the increased speed of MHD jet heads has sometimes been attributed to magnetic pressure in the nose cone. Equation (4.1), however, demonstrates that the increased momentum provided by finite pressure alone cannot account for the enhanced head speed in the MHD cases we have simulated. Using $\eta = 1.5$, $\bar{M}_s \approx 10$, $\bar{M}_a \approx 7$ appropriate to our simulations, this relation gives $v_h = 56$ km s^{-1}, assuming the same head-scale factor $\alpha = 1$ that was used successfully to estimate the jet head speeds for our non-MHD simulations. In fact, the finite pressures nominally add only about 2% to the jet head speeds according to equation (4.1). On the other hand, it is apparent that the tapered shape of the nose cone formed by magnetic hoop stresses has streamlined the flow around the jet head. That effectively increases the geometry factor, α, which can significantly enhance the jet head speed, v_h. From the simulation data we estimate in case D that the radius of the jet head is $R_h \approx 8 \times 10^{15}$ cm, leading to $\alpha^{1/2} \sim 2.5$. Inserting this into equation (4.1) gives a jet head speed of 77 km s^{-1}, closer to the 70 km s^{-1} estimated from the simulation itself.

5. CONCLUSION AND DISCUSSION

The results of these simulations demonstrate that propagation-based diagnostics for radiative MHD jets may exist. The strong effect of magnetic pinches in these axisymmetric calculations change both the structure of the jet head and the beam. The increased velocity of the bow shock is also a distinctive feature of MHD jets. These morphological and kinematic characteristics would alter the observed emission properties in a real YSO jet. The strong shocks in the beam would produce

increased excitation of both atomic and molecular lines. The increased speed of the jet head will alter both the degree of ionization and excitation. This study is too preliminary, however, to provide observers with a definitive accounting of the differences between real radiative hydrodynamic and MHD jets. We leave this task to future studies (Frank et al. 1998).

The most obvious deficit in our models is the imposed axisymmetry. Cerqueira et al. (1997) have recently reported three-dimensional SPH calculations that also show that strong toroidal field components dramatically alter the morphology of the jets, consistent with our results. Their numerical resolution was too low, however, to see the detailed structure of shocks in both the beam and the jet head, which are both clearly captured in our simulations. Since these kinds of structures are not seen in observations, Cerqueira et al. (1997) (who did observe the narrowing of the jet head due to pinch forces) concluded that real YSO jets cannot have significant toroidal fields. If future high-resolution grid-based and SPH-based codes continue to find such effects, that may pose a serious challenge to MHD jet models that rely on collimation via hoop stresses.

It is also worth noting the role of reconnection. The initial conditions used in our models do not allow for field reversals to occur. If a poloidal (B_z) component exists, then field lines embedded in the beam will be decelerated upon passage through the jet shock. If the fields and cooling are not strong enough to inhibit the formation of a cocoon, these lines will be carried backward-forming field reversals (Frank et al. 1997; Kössl et al. 1990b). Such a topology is unstable to resistive tearing mode instabilities and magnetic reconnection. The presence of reconnection in jets could have important consequences for the interpretation of shock emission diagnostics (Hartigan, Morse, & Raymond 1993). Reconnection would provide an alternate means for converting kinetic energy into a thermal energy (the field acts as a catalyst; Jones et al. 1997), which is then channeled into collisionally excited emission.

REFERENCES

Begelman, M. 1997, preprint
Blondin, J. M., Fryxell, B. A., & Königl, A. 1990, ApJ, 360, 370
Borkowski, K., Blondin, J. M., & Harrington, J. 1997, ApJ, 482, 97
Burrows, C., et al. 1996, ApJ, 473, 437
Camenzind, M. 1997, in IAU Symp. 182, Herbig-Haro Flows and the Birth of Low-Mass Stars, ed. B. Reipurth & C. Bertout (Dordrecht: Kluwer), 241
Clarke, D., Norman, M., & Burns, J. 1986, ApJ, 311, L63
Cerqueria, A., de Gouvineia Dal Pino, E., & Herant, M. 1997, ApJ, 489, L185
Dalgarno, A., & McCray, R. 1972, ARA&A, 10, 375
Dal Pino, E., & Benz, W. 1994, ApJ, 435, 261
Franklin, J., Noriega-Crespo, A., & Frank, A. 1996, BAAS, 28, 1341
Frank, A., Balick, B., & Livio, M. 1996, ApJ 471, L53
Frank, A., Jones, T. W., Ryu, D., & Noriega-Crespo, A. 1997, in IAU Symp. 182, Herbig-Haro Flows and the Birth of Low-Mass Stars, ed. F. Malbet & A. Castets (Grenoble: Obs. Grenoble), 115
———. 1998, in preparation

Frank, A., & Mellema, G. 1996, ApJ 472, 684
———. 1997, in IAU Symp. 182, Herbig-Haro Flows and the Birth of Low-Mass Stars, ed. B. Reipurth & C. Bertout (Dordrecht: Kluwer), 291
Hardee, P., Clarke, D., & Rosen, A. 1997, ApJ, 485, 533
Harten, A. 1983, J. Comp. Phys., 49, 357
Hartigan, P., Morse, J., & Raymond, J. 1993, ApJ, 434, 232
Jones, T. W., Gaalaas, J. B., Ryu, D., & Frank, A. 1997, ApJ, 482, 230
Königl, A., & Ruden, S. P. 1993, in Protostars and Planets III, ed. E. H. Levy & J. I. Lunine (Tuscon: Univ. Arizona Press). 641
Kössl, D., Mueller, E., & Hillebrandt, W. 1990a, A&A, 229, 378
———. 1990b, A&A, 229, 397
Lind, K., Payne, D., Meier, D., & Blandford, R. 1989, ApJ, 344, 89
Mellema, G., & Eulerink, F. 1994, A&A, 284, 654
Mellema, G., & Frank, A. 1998, MNRAS, in press
Norman, M. L. 1993, in Astrophysical Jets, ed. D. Burgarella, M. Livio, & C. O'Dea (Cambridge: Cambridge Univ. Press), 210

Ouyed R., & Pudritz, R. E. 1997, ApJ, 482, 712

Ostriker, E. 1997, ApJ, 486, 291

Peter, W., & Eichler, D. 1996, ApJ 466, 840

Priest, E. R. 1984, Solar Magnetohydrodynamics (Dordrecht: Reidel)

Pudritz, R. E. 1991, in The Physics of Star Formation and Early Stellar Evolution, ed. C. J. Lada & N. D. Kylafis (Dordrecht: Kluwer), 365

Raga, A. 1994, Ap&SS, 216, 105

Ray, T., Mundt, R., Dyson, J., Falle, S., & Raga, A. 1996, ApJ, L468

Ray, T., Muxlow, T., Axon, D., Brown, A., Corcoran, D., Dyson, J., & Mundt, R. 1997, Nature, 385, 41

Romanova, M., Ustyugova, G., Koldoba, A., Chechetkin, V., & Lovelace, R. 1997, ApJ, 482, 70

Ryu, D., & Jones, T. W. 1995, ApJ, 442, 228

Ryu, D., Jones, T. W., & Frank, A. 1995, ApJ, 452, 785

Ryu, D., Yun, H., & Choe, S. 1995, J. Korean Astron. Soc., 28, 223

Shu, F., Najiata, J., Ostriker, E., & Shang, H. 1995, ApJ, 495, L155

Shu, F., Najiata, J., Ostriker, E., Wilkin, F., Ruden, S., & Lizano, S. 1994, ApJ, 429, 781

Stone, J. M., & Norman, M. L. 1994, ApJ 413, 198

Suttner, G., Smith, M. D., Yorke, H. W., & Zinnecker, H. 1997, A&A, 318, 595

Todo, Y., Uchida, Y., Sato, T., & Rosner, R. 1992, PASJ, 44, 245

———. 1993, ApJ, 403, 164

Uchida, Y., Todo, Y., Rosner, R., Shibata, K. 1992, PASJ, 44, 227

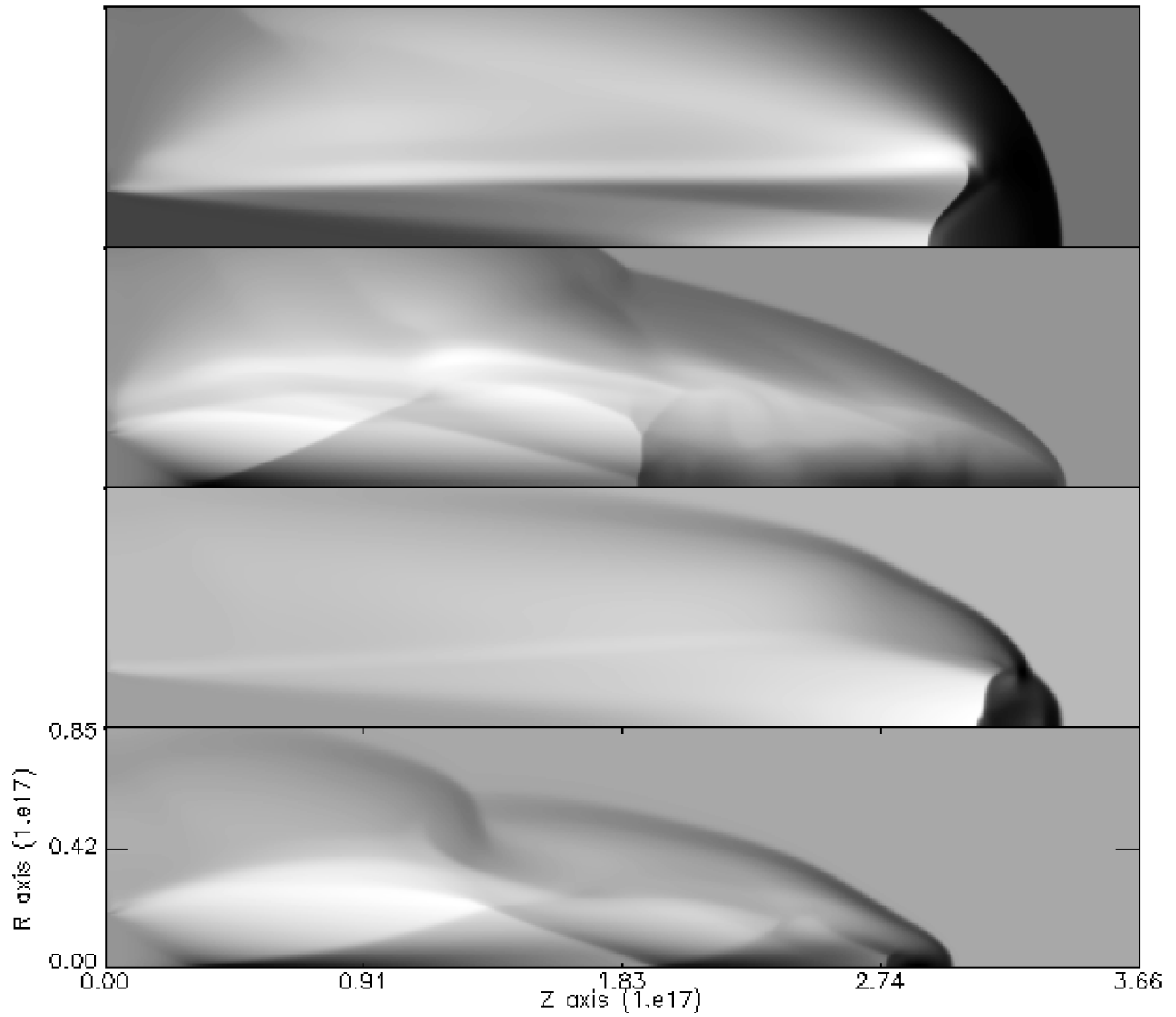Vishniac, E. T. 1994, ApJ, 428, 186

Fig. 1.—Comparison of four YSO Jet simulations; gray-scale log density. (*top*) Weak-field nonradiative ($t = 1971$ yr); (*second from top*) strong-field nonradiative ($t = 1460$ yr); (*third from top*) weak-field radiative ($t = 1971$ yr); (*bottom*) strong-field radiative ($t = 1460$ yr). Note that compression ratios behind bow/jet shocks in the radiative models are higher by 1 order of magnitude compared with the nonradiative cases. Each frame has been autoscaled to its min/max, resulting in different gray-scale ranges.
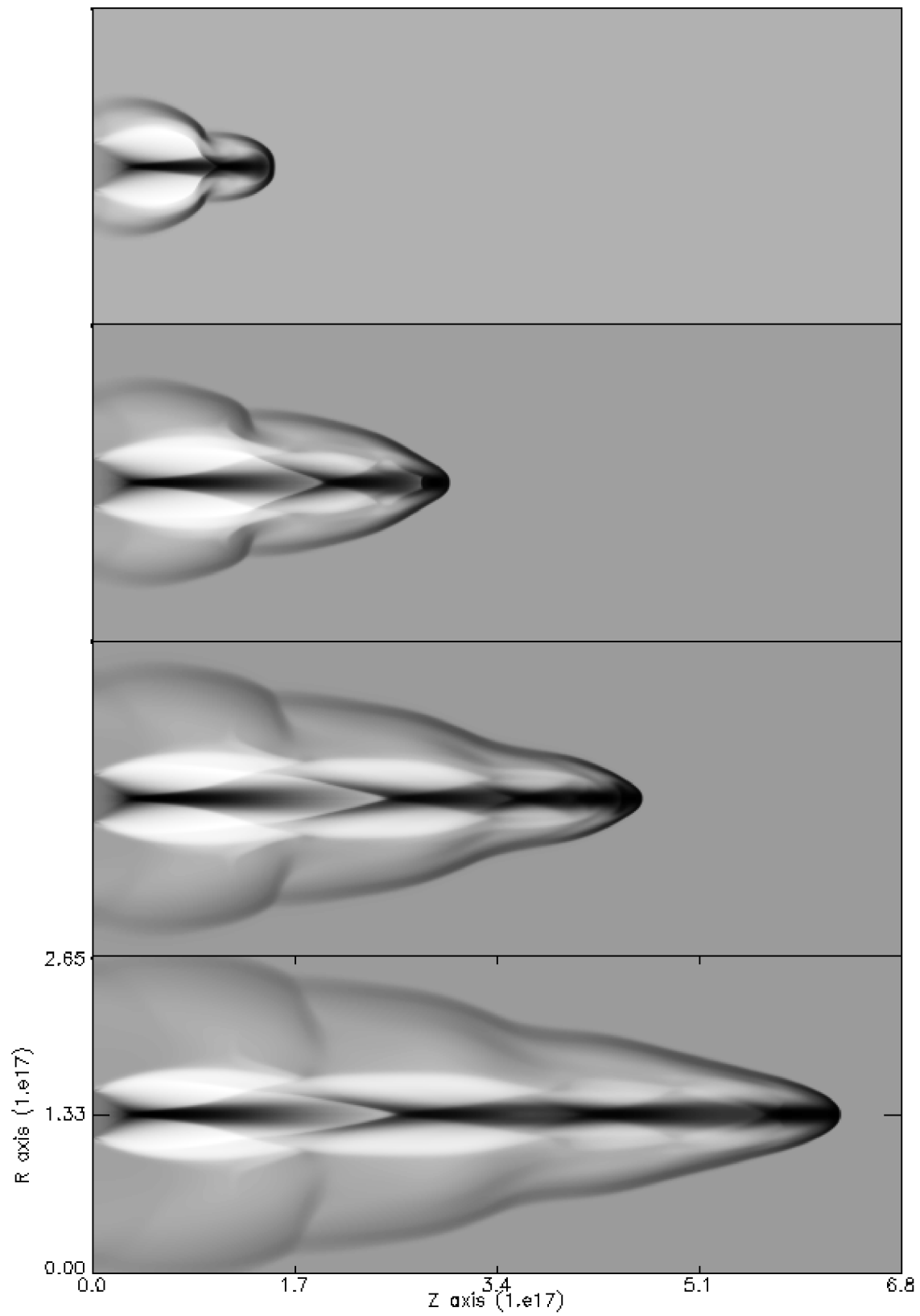
Frank et al. (see 494, L81)

FIG. 2.—Propagation of the radiative strong-field model at 4 times (*from top to bottom*, t = 698, 1398, 2095, and 2793 yr). Each frame has been autoscaled to its min/max resulting in different gray-scale ranges. The min/max values in the frames are approximately 5 and 7000 cm^{-3}.

FRANK et al. (see 494, L81)

PLATE L5